Modeling and Detailed Numerical Simulation of the Primary Breakup of the "Spray G" Gasoline Jet

B. Zhang and Y. Ling*
Department of Mechanical Engineering
Baylor University
Waco, TX 76798 USA

Abstract

In the present work, we model and simulate the injection and atomization of a non-reacting and non-evaporative gasoline surrogate jet by detailed numerical simulation. The nozzle geometry and operation conditions are similar to the Engine Combustion Network (ECN) "Spray G". We focus the present study on the primary breakup in the near field where inter-jet interaction is of secondary importance. Therefore, we have considered only one of the eight jets in the original Spray G injectors. The liquid is injected from the inlet into the stagnant gas chamber. A tangential velocity is added in the inlet to mimic the complex internal flow in the original spray G injector, which leads to the plume deflection. A parametric study on the inlet tangential velocity is carried out to identify the proper value. Simulations are performed with the multiphase flow solver Basilisk on an adaptive mesh. The gas-liquid interface is captured by the volume-of-fluid method. The model and simulation are validated by comparing the computed results of plume angle, penetration speed with experimental data. It is shown that vortices created inside the nozzle influence the near-field primary breakup of the gasoline jet. Due to the larger Reynolds number, the near-field multiphase flow is highly turbulent. The lambda-2 vortex identification criterion is utilized to characterize the vortices dynamics.

 $^{{\}rm *Corresponding\ Author:\ stanley_ling@baylor.edu}$

Introduction

The application of the direct injection in the gasoline engines play an important role in improving the fuel economy and simultaneously reducing the pollutant emission. The gasoline direct injection (GDI) system, being capable of providing accurate fuel delivery and less cycle-to-cycle variation, is critical to the subsequent fuel/air mixing, spark ignition, and flame propagation in the internal engine [1].

The spray atomization is significantly influenced by the injector nozzle geometry. Yue et al. [1] showed that the machine details of the injector could influence the spray development process considerably. Duke et al. [2] investigated the Engine Combustion Network (ECN) "Spray G" gasoline injector, using X-ray tomography, phase doppler interferometry, and laser induced fluorescence by summoning up resources from multiple institutions. They mainly studied the internal and near-nozzle flow.

Befrui et al. [3] took advantage of volume-offluid large-eddy-simulation (VOF-LES) method to study the ECN "Spray G" seat flow and the nearfield primary atomization. Mitroglou et al. [4] characterized the performance of the multi-hole injectors by measuring the spatial and temporal distributions of the droplet velocity and diameter at distinct locations. Aori et al. [5] investigated the effect of nozzle configuration on the macroscopic spray structures of multi-hole fuel injectors under superheated conditions.

The liquid and vapor phases of the spray were captured through DBI and Schlieren imaging for the ECN "Spray G" [6]. The studies of a gasoline direct injection multi-hole injector valve-group and the corresponding plumes with the aid of computational fluid dynamics methods are already performed to investigate the primary breakup of a single plume [7]. The effect of transient needle motion on ECN "Spray G" multi-hole injector's internal and near nozzle flow was studied by the homogeneous relaxation model coupled with the volume-of-fluid approach [8].

In spite of remarkable improvement in both experiments and simulations under standard "Spray G" conditions, a detailed numerical simulation of the spray formation of the galoline liquid jet is still lacking. The detailed numerical simulation can offer high-resolution characterization of the flow field and the spray structures.

In this work, the atomization of a gasoline jet injected under ECN "Spray G" operating condition is investigated by a three dimensional direct numerical simulation in the near-field. One of the eight jets in the original "Spray G" injectors is taken into account for the inter-jet interaction is less important in

the near-field. The adaptive multiphase flow solver Basilisk is applied and the volume of fluid method is used to reconstruct the interface. A tangential component of the injection velocity is added in the inlet to mimic the plume deflection created by the internal geometry of the injector in ECN "Spray G" experiments. It is demonstrated that the flow asymmetry caused by the tangential injection velocity inside the nozzle contributes to the generation and propagation of the turbulent structures in the near field. It is also revealed that the interaction between the turbulence and the interfacial waves initiates a great number of small eddies produced across the jet. The Cartesian effect is ruled out by rotating the direction of the tangential velocity in the inlet 45 degrees with respect to the y axis in the simulation. Moreover, the momentum conservation is studied as well to the computation to account for the high density ratio between the liquid and the ambient gas [9].

The paper is organized as follows. In the next section, we present the numerical modeling and the simulation setup. Then we present the results and the validation of the simulation in Sec. 3.

Numerical Modeling and Simulation Setup Governing Equations

The one-fluid approach is employed to resolve the two-phase flow, where the phases corresponding to the fuel and the ambient air are treated as one fluid with material properties that change abruptly across the interface. The incompressible, variabledensity, Navier-Stokes equations with surface tension can be written as

$$\rho(\partial_t \mathbf{u} + \mathbf{u} \cdot \nabla \mathbf{u}) = -\nabla p + \nabla \cdot (2\mu \mathbf{D}) + \sigma \kappa \delta_s \mathbf{n}, \quad (1)$$
$$\nabla \cdot \mathbf{u} = 0, \quad (2)$$

where ρ , μ , \mathbf{u} , and p represent density and viscosity, velocity and pressure, respectively. The deformation tensor is denoted by \mathbf{D} with components $D_{ij} = (\partial_i u_j + \partial_j u_i)/2$. The third term on the right hand side of Eq. (1) is a singular term, with a Dirac distribution function δ_s localized on the interface, and it represents the surface tension force. The surface tension coefficient is σ , and κ and \mathbf{n} are the local curvature and unit normal of the interface.

The volume fraction C is introduced to distinguish the different phases, in particular C=1 in the computational cells with only the ambient air (respectively C=0 in the fuel), and its time evolution satisfies the advection equation

$$\partial_t C + \mathbf{u} \cdot \nabla C = 0. \tag{3}$$

The fluid density and viscosity are then defined by

$$\rho = C\rho_a + (1 - C)\rho_l \,, \tag{4}$$

$$\mu = C\mu_a + (1 - C)\mu_l. (5)$$

where the subscripts a and w represent the ambient air and the fuel respectively.

$Numerical\ Methods$

The Navier-Stokes equations (Eqs. (1) and (2)) are solved by a novel adaptive multiphase solver Basilisk [10]. In Basilisk, the interface between the different fluids are tracked using a Volume-of-Fluid (VOF) method [11, 12]. A quad/octree spatial discretisation is used, which gives a very important flexibility allowing dynamic grid refinement into user-defined regions. Finally the height-function (HF) method is utilized to calculate the local interface curvature, and a balanced-force surface tension discretization is used [13, 14].

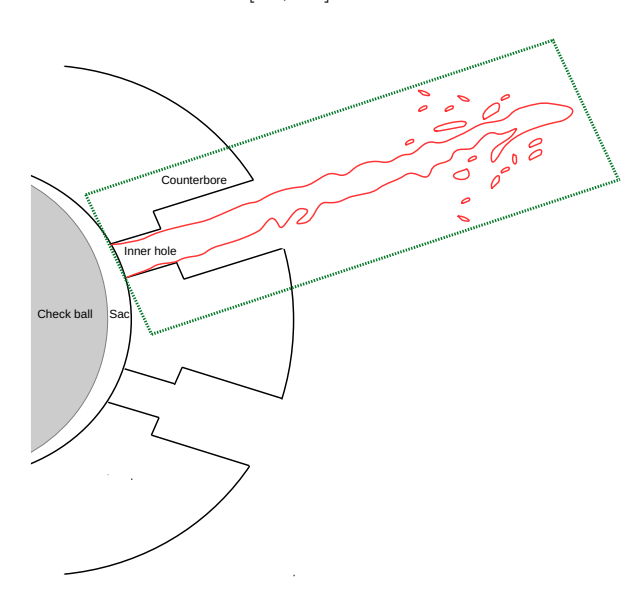


Figure 1. Geometry of the Spray "G" nozzle and the simulation region.

Modeling and Simulation Setup

The geometry of the Spray "G" nozzle is shown in Fig. 1, where the region enclosed by the green rectangle is our interest of simulation. Due to the internal geometry of the nozzle, the tangential components of the injection velocity are created when the jet exits from the inner hole. In order to mimic this flow characteristic, we add a tangential component of the injection velocity along the positive y direction in simulation. In the simulation setup, the fuel is injected into a cubic domain filled with stag-

nant nitrogen gas along the x direction from the left boundary. A large simulation domain is used for this study owing to the octree discretization of Basilisk such that the effects of boundaries to the atomizing jet are negligible. The computational domain for the atomizing jet is shown in Fig. 2. The fluids properties and the injection conditions are chosen based on the Argonne X-ray experiments, where a low-volatility gasoline surrogate with a cerium contrast agent is used [2], see Table 1. Due to the low vapor pressure in the chamber and the use of lowvolatility liquid, evaporation can be ignored in the present simulation. In the numerical method we ignore the internal geometry of the "Spray G" nozzle. A tangential velocity along the positive y direction is then added to the inflow velocity to mimic the deflection of the plume relative to the nozzle axis. The outflow boundary condition is invoked at the right boundary. All the rest boundaries of the domain are then taken as symmetric boundaries. The edge length of the domain is 64 R_{inj} , where R_{inj} is the inner nozzle radius. The minimum cell size of the adaptive mesh used is indicated by Δ_{\min} , which is equal to 5.4 μ m. A snapshot of the atomizing jet and the corresponding adaptive mesh are shown in Fig. 2. It is easily seen that high mesh resolution is used to resolve the liquid-gas interface while the mesh away from the jet is coarsen to decrease computational costs. The total number of cells increases in time as more liquid is injected into the domain. The mesh shown in Fig. 2, which is a snapshot corresponding to $tU_{inj}/R_{inj}=23$, consist of about 16 million cells. The liquid normal injection velocity $U_{inj}/R_{inj} = 89$ m/s used in the present study is identical to that used in the standard "Spray G" operating conditions.

Results

Evolution of the Gasoline Jet

Following the experiments of Duke et al. [2], the gas in the chamber is nitrogen, with a pressure and temperature of 3.15 bar and 298 K, respectively. The density and viscosity of the gas are 3.6 kg/m^3 and 1.77×10^{-5} Pa s, respectively. If the gas density, the jet radius, and the injection velocity are chosen to be reference scales, the key dimensionless parameters can be calculated, see Table 2. The Reynolds and Weber numbers of the liquid jet are defined as $\text{Re}_l = \rho_l(2R_{inj})U_{inj}/\mu_l$ and $\text{We}_l = \rho_l(2R_{inj})U_{inj}^2/\sigma$, respectively, which characterize the inertial effect compared to the viscous and surface tension forces. When Re_l and We_l are large, the viscous and surface tension forces are insufficient to hold the injected fuel as a bulk liquid, resulting

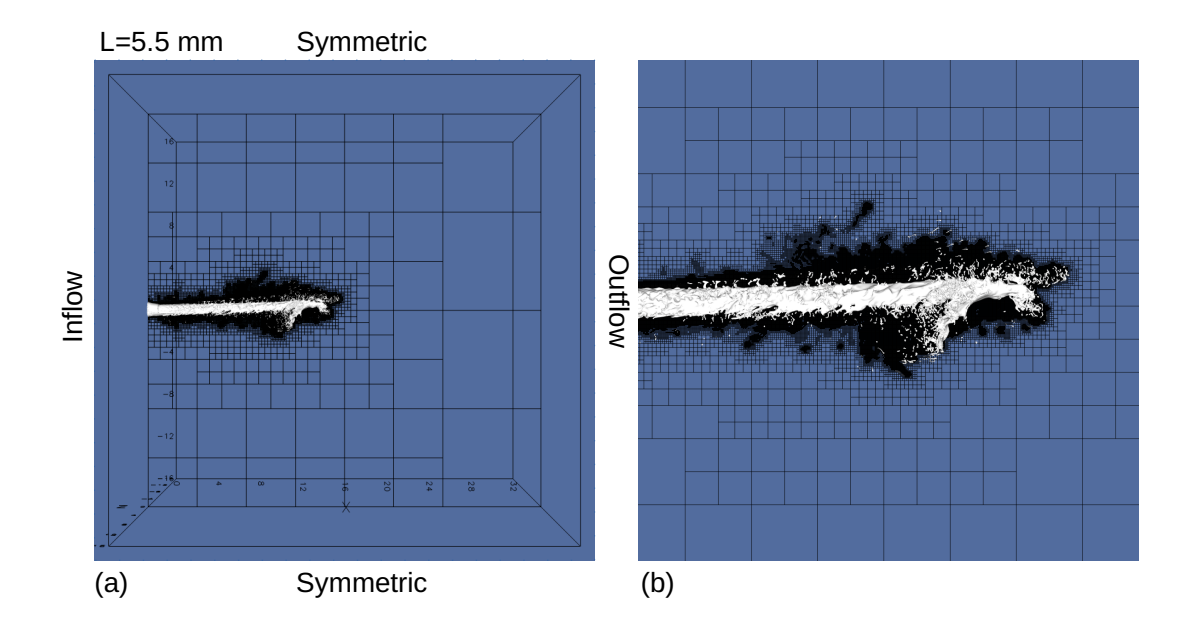


Figure 2. Simulation setup for an atomizing gasoline jet (a) and the adaptive mesh utilized (b).

Fuel	$gasoline\ calibration\ fluid$	
Density ρ_l	838 kg/m^3	
Viscosity μ_l	$9.64 \times 10^{-4} \text{ Pa s}$	
Surface tension σ	$0.0278 \; \mathrm{N/m}$	
Jet radius R_{inj}	$8.65 \times 10^{-5} \text{ m}$	
Normal injection velocity U_{inj} 89 m/s		
Tangential injection velocity V_{inj}	0, 17.8, 35.6 m/s	
A 7 · /	37	
Ambient gas	N_2	
<i>D</i>	0.61 / 3	
Density ρ_g	3.6 kg/m^3	
Viscosity μ_g	$1.77 \times 10^{-5} \text{ Pa s}$	

Table 1. Fuel properties and injection parameters.

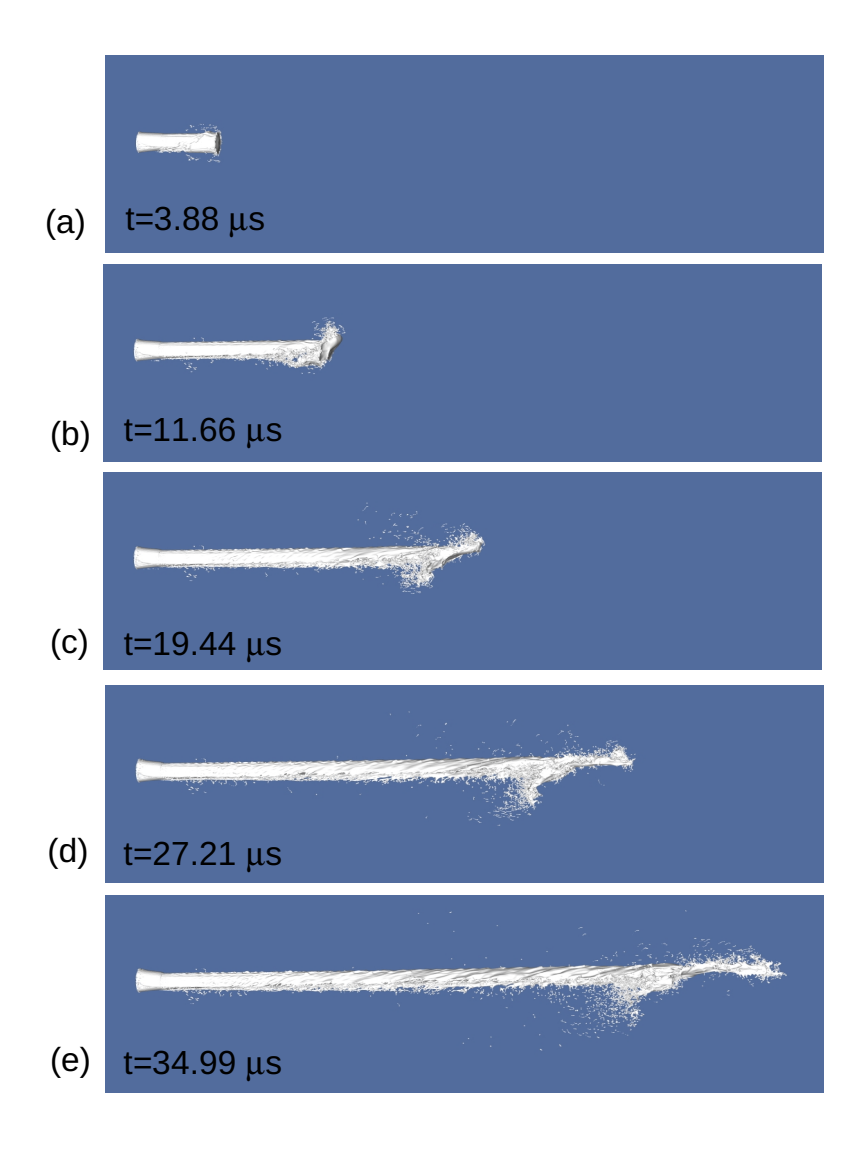


Figure 3. Evolution and disintegration of the gasoline jet.

Re_g	Re_l	We_l	r
3.13×10^{3}	1.34×10^{4}	4.13×10^{4}	2.33×10^{2}

Table 2. Key dimensionless parameters.

in atomization of the liquid jet into smaller droplets. As the gas flow is generated by the injected liquid in the chamber, the Reynolds number in terms of the gas properties, $\text{Re}_g = \rho_g(2R_{inj})U_{inj}/\mu_g$, is utilized to measure the induced gas flow. When Re_g is big enough the gas flow can become turbulent. Finally, the liquid-to-gas density ratio is represented by r with $r = \rho_l/\rho_g$. Other dimensionless parameters can be computed based on these four parameters, for example, the liquid-to-gas viscosity ratio is equal to $r\text{Re}_g/\text{Re}_l$.

In this section, the in-nozzle flow effects due to both the nozzle geometry and the added tangential velocity $(V_{inj} = 17.8 \text{ m/s})$ on the jet evolution and atomization are presented. The jet is injected into the stagnant nitrogen gas and a mushroom head is formed (see Fig. 3 (a)). As the jet advects downstream, the asymmetry created by the tangential velocity on the liquid jet caused the jet head to tilt upward, as shown in Figs. 3 (b)-(f). With the flow progressing, the mushroom head grows and the tilted head part translates faster and is thus extended further along the streamwise direction. The head dynamics dominates the droplets generation process and there are also droplets disintegrated from the jet core. The Kelvin-Helmholtz instability developing at the liquid-air interface due to the shear induced circumferential waves around the jet, which contributes to the primary breakup of the gasoline jet. The instability created by the tangential velocity of the injected jet enhances the Kelvin-Helmholtz instability and subsequently initiates asymmetric surface waves propagating on the top region of the jet [Figs. 3 (c) and 3 (d)], which makes ligaments pinch off from the jet top region when the jet progresses downstream (see Fig. 3 (e)) and as the jet advects further the as-produced filaments breaks up into droplets [Figs. 3 (f)]. The turbulence developed in the flow field plays a part in disintegrating the liquid jet as well.

Parametric Study

A parametric study by varying the tangential velocity in the inlet is performed. As seen in Fig. 4 (a), a good agreement of the jet penetration between the experiment and simulation can be achieved when $U_t = 17.8 \,$ m/s. When the tangential velocity in-

creases, the jet penetration speed increases due to the increase of the total injection velocity. Simultaneously, the jet deflects from its normal trajectory along the streamwise direction towards the spanwise direction owing to the added tangential component of the velocity. The vectoring of the plume angle with respect to the drill angle increases by increasing the tangential velocity, see Fig. 4 (b). The plume angle deviation from the drill angle is around 2 degrees and agrees well the experimental result by comparing Fig. 4 (b) with that of Fig. 13. (a) in Ref. [2]. The noises in plume angle evolution is the instabilities at the jet interfaces. The fluctuation's amplitude increases with the increase of the magnitude of the tangential velocity.

Near-Field Flow Dynamics

Three simulation setups are employed to study the flow field and liquid structures of the gasoline jet penetration. Setup 1 corresponds to adding the tangential velocity along the positive y direction, while setup 2 and 3 correspond to adding the tangential velocity along the direction having 45 degrees with both the positive y and z directions in the y-z plane. Setup 2 does not take into account momentum conserving, but setup 3 does.

As seen in Fig. 6, due to the Cartesian effect, a "fin" is formed on the top of the jet and the instability develops along the "fin" for setup 1. This "fin" vanishes if we get rid of the Cartesian effect by rotating the added tangential velocity 45 degrees from the positive y towards positive z direction, see setup 2 and 3. The liquid breaks up more violently with adding the momentum conserving for setup 3. When time elapses and jet head advects downstream, the liquid core in the near-field achieves a relatively steady state.

The second invariant of the velocity gradient tensor λ_2 vortex-identification criterion with a value of -1, colored by the streamwise velocity, is applied to demonstrate the evolution of the coherent vortical structures and the influence of turbulence on the liquid atomization. Due to the high Reynolds number, a turbulent jet is formed once the liquid is injected into the computational domain from the inner nozzle. See Fig. 7.

As shown in Fig. 7, the gasoline jets exhibit similar vortical structures for setup 1 and 2, where a lot of deformed vortex tubes are formed along the jet core. However, less vortical structures are created for setup 3. As time passes, more vortices are created in the jet core for setup 3.

The three setups share some similar flow behaviors. The in-nozzle turbulent structures are prop-

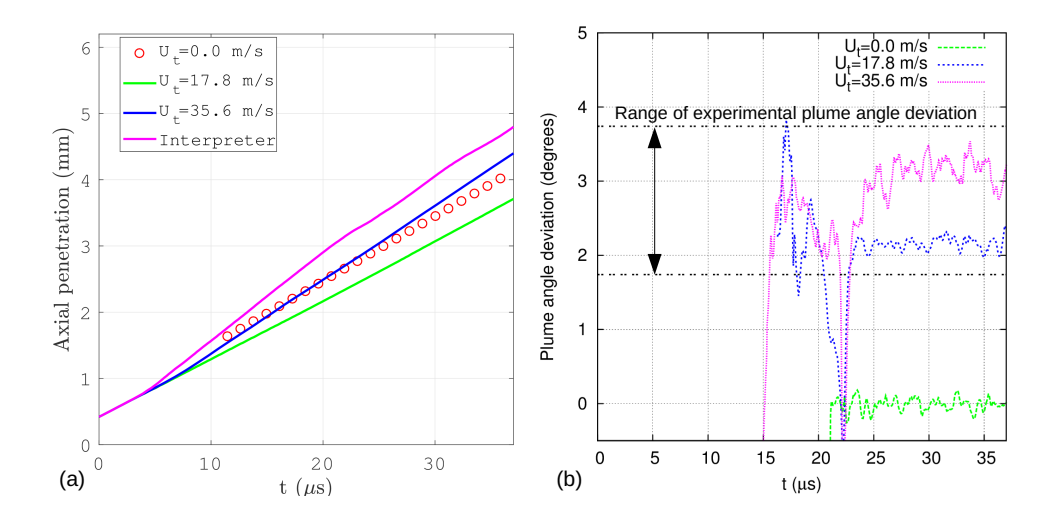


Figure 4. Gasoline liquid jet penetration measured from the present simulation with distinct tangential velocities and previous experimental work of Ref. [2] (a) and the plume angle deviation from the drill angle (b).

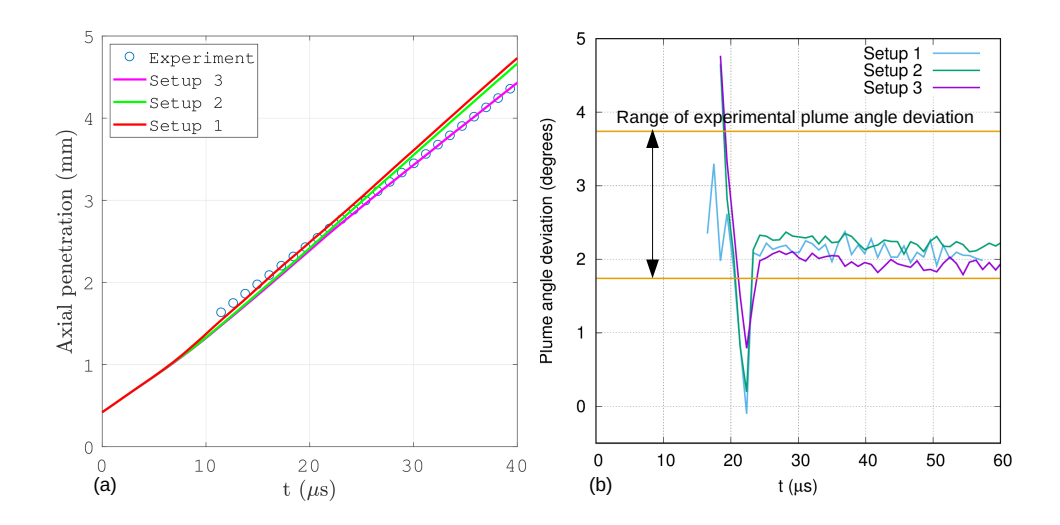


Figure 5. Gasoline liquid jet penetration measured from the present simulation with distinct tangential velocities and previous experimental work of Ref. [2] (a) and the plume angle deviation from the drill angle (b).

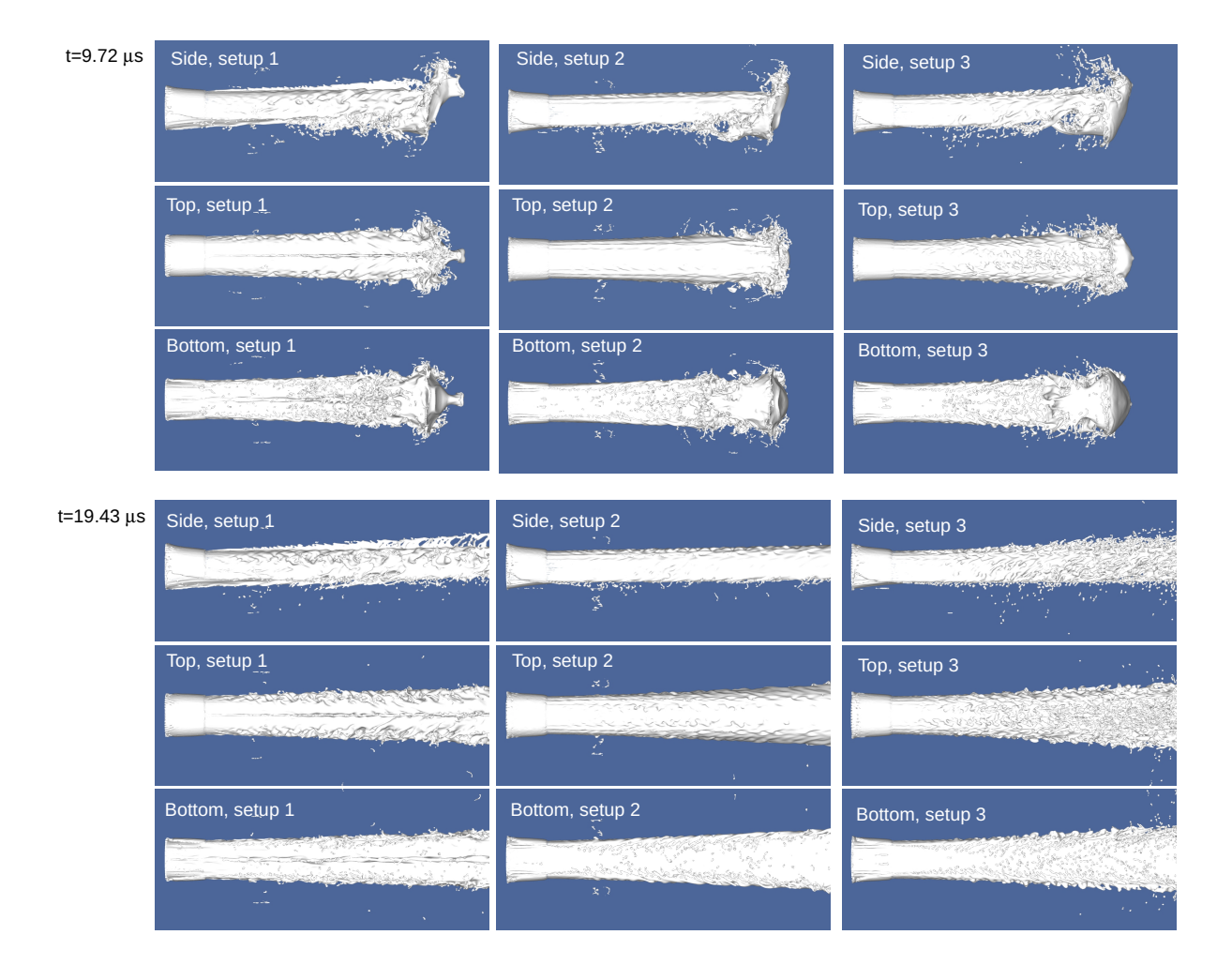


Figure 6. Comparing the evolution of the volume of fluid isosurfaces from different views for the gasoline liquid jet penetration with three distinct setups.

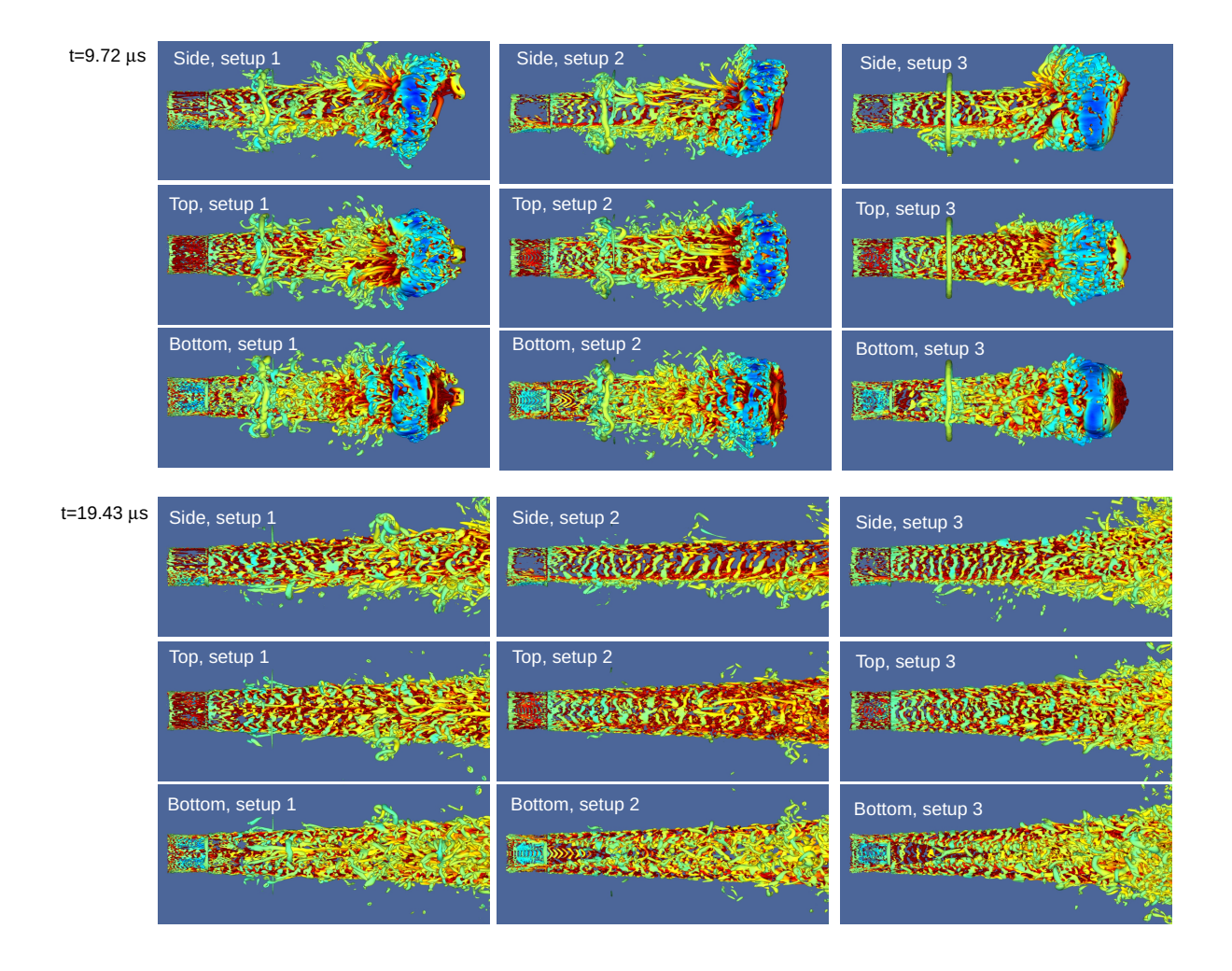


Figure 7. Comparing the evolution of the lambda-2 isosurfaces colored by the streamwise velocity magnitude from different views for the gasoline liquid jet penetration with three distinct setups.

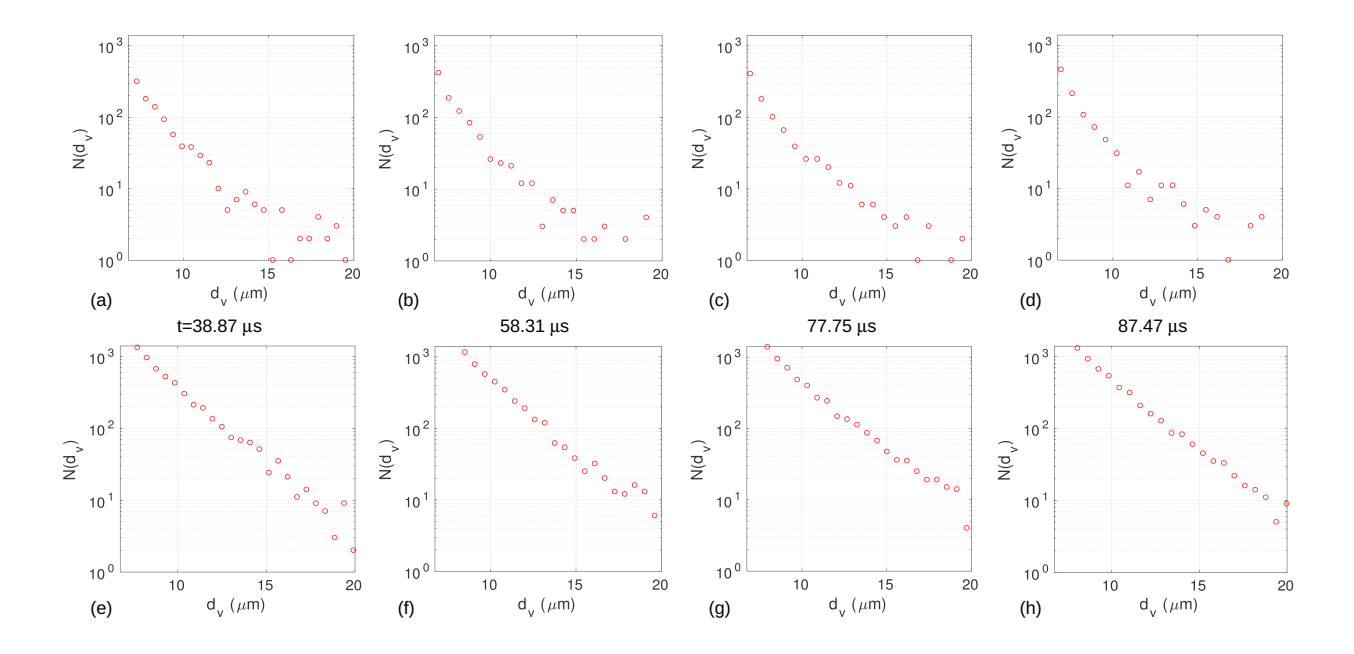


Figure 8. Evolution of droplet size distribution for setup 2 (a-d) and setup 3 (e-h).

agated away from the nozzle and interact with the interfacial Kelvin-Helmholtz waves, enhancing the interfacial disturbances and contributing to the jet atomization. The ambient gas is entrained into the counterbore due to the lower pressure created inside the counterbore, which is induced by the fast flowing liquid. Simultaneously, the azimuthal asymmetry created by the tangential velocity caused further entrainment of the surrounding gas into the bottom wall of the inner-nozzle, which shifts the jet upwards and induces a flow constriction and a further narrowed jet. The entrainment of the gas into the nozzle generates more vortices subsequently.

The longitudinal vortical structures are formed along the jet core and stretched by the pull of the strong interfacial aerodynamic force. As the flow progresses, more vortices are generated in the nearfield owing to the turbulent jet and the turbulence in the moving gas induced by the disturbing jet. The spanwise vortical structures are developed close to the jet head. Furthermore, the hairpin vortices are created from the jet head and are pulled by the gas and flow backward along the longitudinal direction. As the jet advects further downstream, more turbulent structures are produced close to the jet and spread up from the jet region into the gas.

Drop Statistics

Fig. 8 shows the temporal evolution of the distribution of droplet number over the droplet volume-based diameter for setup 2 and 3. Figs. 8 (a)-(d) and

(e)-(h) indicate that more droplets are generated for setup 3 at each stage. For both cases, the dominant droplet size is 6.7 μ m and in this simulation the droplets with a diameter less than 6.7 μ m have been removed during simulation. The linear relations in all plots indicate that the droplet sizes obey an exponential distribution for both setup 2 and 3 at different time.

Conclusions

The penetration and atomization of a gasoline liquid jet are investigated in the near-field in the present work. A parametric study based on varying the tangential component of the injecting velocity is performed initially to mimic the deflection of the fuel plume from the nozzle axis in the experiments under "Spray G" conditions, which gives a reasonable tangential velocity. The simulated penetration and vectoring of the plume are found to agree well with the Argonne X-ray experiments. Furthermore, the low-volatility of the gasoline surrogate utilized in Argonne X-ray experiments validates the application of the current code without considering the vapor phase.

Three distinct setups are considered and the momentum conserving code is used.

The in-nozzle turbulence enhances the disintegration of the liquid jet and contributes to the fragmentation of the liquid filaments by the propagation of the induced disturbances along the jet. The hairpin vortices are easily distinguished and the evolution of the vortical structures can be conveniently traced with the application of the λ_2 vortex identification criterion.

The drop statistics is studied, which reveals that the drop size distribution follows an exponential law.

Acknowledgements

This work was supported by Baylor University. The simulations were performed on the Baylor cluster *Kodiak* and Texas Advanced Computing Center cluster *TACC*.

References

- [1] Z. Yue, M. Battistoni, and S. Som. Fourteenth International Conference on Liquid Atomization and Spray Systems, Chicago, IL, USA, July 2018, 2018.
- [2] D. J. Duke, A. L. Kastengren, K. E. Matusik, A. B. Swantek, C. F. Powell, R. Payri, D. Vaquerizo, L. Itani, G. Bruneaux, R. O. Grover Jr, S. Parrish, L. Markel, D. Schmidt, J. Manin, S. A. Skeen, and L. M. Pickett. *Exp. Therm.* Fluid Sci., 88:608–621, 2017.
- [3] B. Befrui, A. Aye, A. Bossi, L. E. Markle, and D. L. Varble. *ILASS Americas 28th Annual Conference, Dearborn (MI)*, USA, pp. 304–316, 2016.
- [4] N. Mitroglou, J. M. Nouri, Y. Yan, M. Gavaises, and C. Arcoumanis. SAE Technical Paper, 2007.
- [5] G. Aori, D. Hung, M. Zhang, G. Zhang, and T. Li. *Atomization sprays*, 26(5), 2016.
- [6] R. Payri, F. J. Salvador, P. Martí-Aldaraví, and D. Vaquerizo. Appl. Therm. Eng., 112:304–316, 2017.
- [7] B. Befrui, G. Corbinelli, M. D'Onofrio, and D. Varble. SAE Technical Paper, 2011.
- [8] B. Mohan, M. Jaasim, F. H. Perez, J. Sim, W. Roberts, and H. Im. Proceedings of the 10th International Symposium on Cavitation (CAV2018), 2018.
- [9] D. Fuster, M. Arrufat, T. and Crialesi-Esposito, Y. Ling, L. Malan, S. Pal, R. Scardovelli, G. Tryggvason, and S. Zaleski. arXiv:1811.12327, 2018.
- [10] S. Popinet. The basilisk code. Available from http://basilisk.fr/.
- [11] R. Scardovelli and S. Zaleski. Annu. Rev. Fluid Mech., 31:567–603, 1999.

- [12] G. Tryggvason, R. Scardovelli, and S. Zaleski. Direct numerical simulations of gas-liquid multiphase flows. Cambridge University Press, 2011.
- [13] M. M. Francois, S. J. Cummins, E. D. Dendy, D. B. Kothe, J. M. Sicilian, and M. W. Williams. J. Comput. Phys., 213:141–173, 2006.
- [14] S. Popinet. J. Comput. Phys., 228(16):5838–5866, 2009.